Resonance trapping and saturation of decay widths

E. Persson, T. Gorin, and I. Rotter*
Max-Planck-Institut für Physik Komplexer Systeme, D-01187 Dresden, Germany
and Technische Universität Dresden, Institut für Theoretische Physik, D-01062 Dresden, Germany
(Received 17 November 1997; revised manuscript received 23 March 1998)

Resonance trapping appears in open many-particle quantum systems at high level density when the coupling to the continuum of decay channels reaches a critical strength. Here a reorganization of the system takes place and a separation of different time scales appears. We investigate it under the influence of additional weakly coupled channels as well as by taking into account the real part of the coupling term between system and continuum. We observe a saturation of the mean width of the trapped states. Also the decay rates saturate as a function of the coupling strength. The mechanism of the saturation is studied in detail. In any case, the critical region of reorganization is enlarged. When the transmission coefficients for the different channels are different, the width distribution is broadened as compared to a χ^2_K distribution where K is the number of channels. Resonance trapping takes place before the broad state overlaps regions beyond the extension of the spectrum of the closed system. [S1063-651X(98)00208-6]

PACS number(s): 05.30.−d, 03.65.Nk, 24.30.−v, 82.30.−b

I. INTRODUCTION

At low excitation energy, the states of a many-particle quantum system are usually well isolated from one another. Their coupling via the continuum of decay channels can therefore be neglected. The reaction cross section consists of a sum of resonances with Breit-Wigner shapes the positions, widths, and partial widths of which are well defined.

At higher excitation energy both the level density and the decay widths of the states in most systems become so large that the resonance states overlap. The cross section is an interference picture. Neither the positions, the widths, nor the partial widths of the resonance states can unambiguously be determined from an analysis of the cross section, see, e.g., [1]. Meaningful values can be obtained from time measurements which provide the average lifetime of the resonance states at high level density. Using the channeling method, the mean lifetime of fine structure resonances under isobaric analog resonances in medium nuclei was found experimentally to be much longer than expected on the basis of the statistical theory of nuclear reactions [2]. The modification of the Fano profiles of autoionizing states due to the coherent coupling with each other has been studied experimentally by means of the two states $3p^2\ ^1S$ and $3p3d\ ^1P$ in magnesium atoms [3].

Theoretically, the transition from low to high level density is studied recently in different papers for different systems, see [1,4–26]. As a function of $\overline{\Gamma}/D$ (where $\overline{\Gamma}$ is the average value of the widths of all resonance states, being a measure for the coupling strength of the system to the continuum, and D is the mean level distance) all results show the same characteristic features: beyond a critical value of $\overline{\Gamma}/D$, separated time scales exist when the number of channels is smaller than the number of resonance states. The very existence of different time scales at high level density corresponds to the basic assumption of the unified theory of nuclear reactions formulated phenomenologically about 40 years ago by Feshbach [27] for many resonances coupled to a small number of common decay channels.

The main differences in the results of the different theoretical approaches consist in the behavior of the long-lived resonance states as a function of further increased $\overline{\Gamma}/D$. While the widths saturate in the more realistic models for many-body systems, e.g. [14], they decrease in the random matrix models. A saturation of the decay rates is observed also in the ''bottleneck'' picture of transition state theory which relates the saturation value to the number of independent decay channels rather than to the widths of individual resonance states of the system [28]. As a reply to [29], the mechanism of the saturation is shown by the same authors to be associated with a broadening of the distribution of resonance widths [30]. A broadening of the width distribution at high level density is found also, e.g., in [18,24] and shown in [9,10,16,21,22,26] to be caused by resonance trapping which is the basic process of the redistribution of the system. It leads ultimately to the formation of different time scales.

In this paper we study in detail the widths of the long-lived states as a function of the coupling strength to the continuum since this is a controversial point of discussion. Most calculations are performed beyond the standard random matrix approach.

In Sec. II the phenomenon of resonance trapping is described in the framework of the random matrix theory. The widths of the trapped resonance states do not saturate with increasing coupling strength to the continuum. In Sec. III the spectroscopic values of an open many-particle quantum system are given. Additional terms in the effective Hamiltonian appear which may prevent the widths of the trapped resonance states from decreasing with increasing coupling to the continuum. In the following sections, we discuss the influence of additional terms in the effective Hamiltonian on the widths of the long-lived trapped states. Additional weakly coupled channels are shown to cause a saturation of the mean

*Electronic addresses: persson@mpipks-dresden.mpg.de, gorin@mpipks-dresden.mpg.de, rotter@mpipks-dresden.mpg.de

width with further increasing coupling strength (Sec. IV). The sharp distinction between short- and long-lived states is removed by the real part of the coupling term to the continuum (Sec. V). In both cases, further avoided crossings appear and the biorthogonality of the eigenfunctions of $H^{\rm eff}$ continues to be essential. That means the critical region where the redistribution takes place is enlarged. This can be seen also in the width distribution of the trapped states, investigated in Sec. VI. Some conclusions on the broadening of the width distribution, the separation of time scales, and the saturation of decay rates at high level density are drawn in the last section.

II. RANDOM MATRIX THEORY AND RESONANCE TRAPPING

A. Basic equations

In order to describe resonance phenomena at high level density in a small energy interval far from thresholds the random matrix theory has been developed. The effective Hamiltonian is (see, e.g., [31,6,7])

$$H^{\rm eff}_{\rm RMM}=H_b-iW=H_b-\frac{i}{2}VV^T. \tag{1}$$

Here V is an energy-independent random matrix consisting of K random vectors of dimension N with matrix elements V^c_R. The value $V^2_c=\Sigma^N_{R=1}(V^c_R)^2$ gives the coupling strength of the system to the channel c. Each vector V_c has Gaussian distributed elements with mean value 0 and variance V^2_c/N. H_b is chosen from the Gaussian orthogonal ensemble (GOE) and the mean level density follows a semicircle law. In our case the length of the spectrum is $L=2$ units and therefore the mean level distance in the middle of the spectrum is given by $d=\pi/(2N)$.

According to [32,33], one can obtain the mean width $\langle\Gamma_l\rangle$ of the long-lived resonance states by considering the diagonal elements of the S matrix, averaged over a sufficiently large energy interval. It holds that

$$\prod_{c=1}^{K}|\langle S_{cc}\rangle|=e^{-\pi\langle\Gamma_l\rangle/d}. \tag{2}$$

The mean width $\langle\Gamma_l\rangle$ of the states in the middle of the spectrum is

$$\langle\Gamma_l\rangle=-\frac{d}{2\pi}\sum_{c=1}^{K}\ln(1-\tau_c), \tag{3}$$

where the τ_c are the transmission coefficients, defined as

$$\tau_c=1-|\langle S_{cc}\rangle|^2. \tag{4}$$

These coefficients are calculated in [34] using a resummation method in the power series expansion of the transfer matrix. The result is

$$\tau_c=\frac{4x_c}{(1+x_c)^2},\quad x_c=\frac{\pi V_c^2}{2Nd}. \tag{5}$$

The mean width $\overline{\Gamma}$ of *all* resonance states can be obtained directly from Eq. (1),

$$\overline{\Gamma}=\frac{2}{N}\,{\rm Im}\{{\rm tr}\,H^{\rm eff}_{\rm RMM}\}=\frac{1}{N}\sum_c V_c^2=\frac{2d}{\pi}\sum_c x_c. \tag{6}$$

The parameters x_c measure the coupling strengths of the system to the different decay channels c. For increasing total coupling they subsequently pass over the critical value one. Here the corresponding transmission coefficient reaches its maximal value $\tau_c=1$. The logarithm in Eq. (3) diverges and Eq. (3) loses its validity. Equation (5) is symmetric with respect to an exchange of x_c by $1/x_c$. As a consequence the transmission coefficients do not distinguish between weak and strong total coupling strength. We have $\tau_c<1$ for all $x_c\neq 1$.

In the following sections we will see that at each of the points $\tau_c=1$ a single resonance state separates in width from the remaining ones. For $x_c>1$ this state becomes much broader than the other ones and can no longer be described statistically together with the long-lived resonance states. The width of the short-lived state is [11,25]

$$\Gamma_s=\frac{2Nd}{\pi}\left(x_c-\frac{1}{x_c}\right)=\left(x_c-\frac{1}{x_c}\right),\quad x_c>1 \tag{7}$$

while the widths of the long-lived states decrease as $1/x_c$.

B. Resonance trapping at strong coupling

One interesting question is how the system described by the Hamiltonian $H^{\rm eff}_{\rm RMM}$ behaves as the coupling to the continuum increases. To investigate this question, we replace V by αV in the term W of the effective Hamiltonian, Eq. (1), and vary α.

For small α we can treat W as a small perturbation on H_b. The rank of H_b is N. $H^{\rm eff}_{\rm RMM}$ thus describes N states with energies determined by the eigenvalues of H_b. The widths are proportional to α^2. This holds well as long as the resonances are nonoverlapping.

For large α we can treat H_b as a small perturbation on W. As W has rank K it directly follows that only K states have large widths, see, e.g., [6,7]. The widths of the remaining $N-K$ states are small. That means two different time scales exist.

In this subsection we first illustrate the phenomenon of resonance trapping for N resonance states coupled to the $K=1$ open decay channel. We define

$$\kappa^j=\frac{2}{N-j}\sum_{R=j+1}^{N}\frac{\Gamma_R}{D_0}=2\,\frac{\overline{\Gamma}_{N-j}}{D_0}. \tag{8}$$

Here the sum runs over all but the j broadest states. $D_0=L/(N-1)$ is the mean level spacing of the eigenvalues of H_b and L is the length of the spectrum. For $N-j\gg 1$ the difference between κ^{j-1} and κ^j is $2\Gamma_j/[D_0(N-j)]$ (states ordered according to decreasing width). Further we define

$$\kappa^{\rm tot}=\kappa^{j=0}=\frac{2}{N}\sum_{R=1}^{N}\frac{\Gamma_R}{D_0}=2\,\frac{\overline{\Gamma}}{D_0}. \tag{9}$$

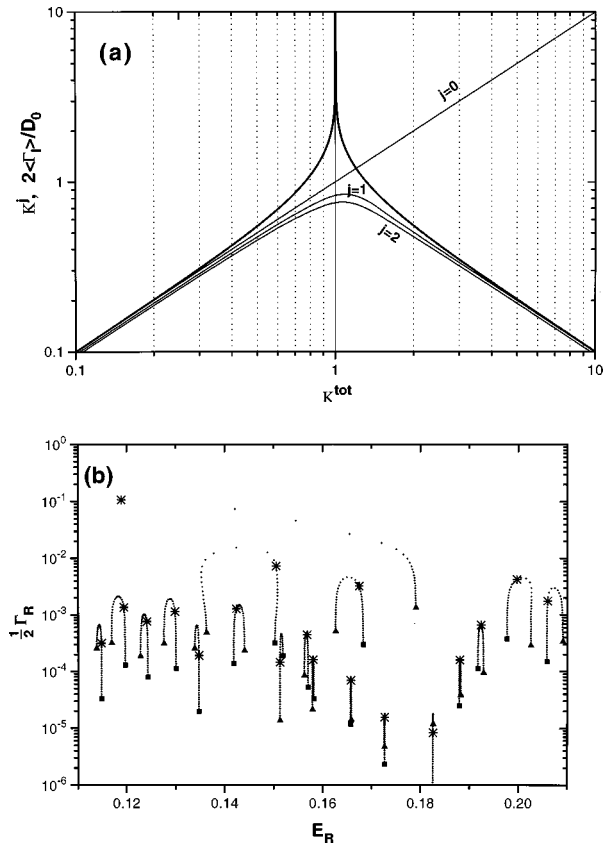

FIG. 1. κ^j for $j=0,1,2$, and $2\langle\Gamma_l\rangle/D_0$, calculated from Eq. (3) (thick line), versus κ^{tot} (a). Eigenvalue picture ($\frac{1}{2}\Gamma_R$ and E_R) calculated for different κ^{tot} (b). The calculation shown is performed within the RMM for $K=1$ and $N=300$. In (a) the curves shown are averages over 20 calculations. Only a part of the spectrum is shown in (b). Note the logarithmic scales. The points for $\kappa^{\mathrm{tot}}=0.1$, 1, and 10 are marked in (b) with triangles, stars, and squares, respectively.

κ^{tot} is a measure of the total coupling strength of the system to the continuum [see Eq. (6)]. In the random matrix theory (with N large) we have $d=\pi/(2N)$ and $L=2$ and thus $D_0=4d/\pi$ which gives $\kappa^{\mathrm{tot}}=x_c$ in the one-channel case (compare Sec. II A).

Within the random matrix theory, we calculate κ^j versus κ^{tot} for $N=300$, $K=1$, and $j=0,1,2$ with varying coupling to the continuum [Fig. 1(a)]. The curves shown are averages over 20 calculations. Note the logarithmic scales. Until $\kappa^{\mathrm{tot}}\approx 1$ the average width of all states increases with increasing coupling to the continuum. At $\kappa^{\mathrm{tot}}\approx 1$ two globally separated time scales are formed. The broad state should be identified with a doorway state [13] and a tight transition state [35], respectively. At the separation point $\kappa^{\mathrm{tot}}=1$, the transmission coefficient is $\tau_c=1$. For still further increasing κ^{tot} the broadest state is getting a still larger width but the average width of the remaining ones decreases.

The thick line in Fig. 1(a) shows $2\langle\Gamma_l\rangle/D_0$ obtained from Eqs. (3) and (5). For $\kappa^{\mathrm{tot}}<1$, $\langle\Gamma_l\rangle$ is the mean width of all N resonance states, $\langle\Gamma_l\rangle\approx\overline{\Gamma}$, while for $\kappa^{\mathrm{tot}}>1$, $\langle\Gamma_l\rangle$ is the mean width of the $N-1$ trapped states, $\langle\Gamma_l\rangle\approx\overline{\Gamma}_{N-1}$. Therefore the transmission coefficients τ_c related to the $\langle\Gamma_l\rangle$ by Eq. (3) do not give us information on the coupling strength κ^{tot} of the system to the continuum (compare Sec. II A).

Resonance trapping of many states takes place whenever the local level density compared to the local mean width is sufficiently large, see, e.g., [14,16,21].

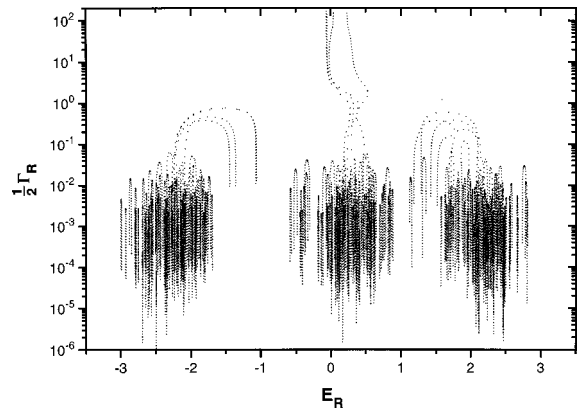

FIG. 2. Eigenvalue picture ($\frac{1}{2}\Gamma_R$ and E_R) for H_b consisting of a sum of three Gaussian shapes. $N=300$, $K=4$, and all channels are coupled with the same strength.

To illustrate the local properties of resonance trapping we show in Fig. 1(b) the widths Γ_R versus the energies E_R for the states of Fig. 1(a). Only a small part of the spectrum is shown. The calculations are performed for $0.1\leqslant\kappa^{\mathrm{tot}}\leqslant 10$ in steps of $\log_{10}(\kappa^{\mathrm{tot}})=0.04$. The points for $\kappa^{\mathrm{tot}}=0.1$, 1, and 10 are marked with triangles, stars, and squares, respectively. As a function of α the complex eigenvalue $\varepsilon_R=E_R-\frac{1}{2}\Gamma_R$ of each resonance state follows a certain ''trajectory.'' For small coupling to the continuum, the widths of the states increase with increasing continuum coupling. This process takes place for every resonance state up to that value of the continuum coupling at which the state starts to overlap one of the resonance states in its neighborhood. The crossing of resonance states is avoided in the complex plane: The states attract each other in energy and their widths bifurcate, i.e., the width of one of the states continues to grow with further increasing coupling strength while that of the other one decreases. The state finally being the broadest one goes through a number of ''collisions'' (avoided resonance crossing between two states looks like a ''collision'' in this representation) before it dominates the complete spectrum. It is formed in the middle of the spectrum where the level density is the largest.

The stars on the trajectories [Fig. 1(b)] show that trapping of resonance states is a local process which takes place *before* different time scales are formed globally. The widths of all the trapped states decrease with further increasing coupling strength.

This behavior does not change when the level density has a band or shell structure. We simulate such a situation by choosing a H_b, Eq. (1), with several more or less separated regions of high level density. Between them and at the borders of the spectrum, the level density is smaller. In the present calculation we have $K=4$ and $N=300$. The coupling of each state to each channel is randomly chosen, i.e., the coupling strengths of the four channels are equal to one another. We have three regions with Gaussian shaped level density. Two of the regions are close to each other and the third one is lying well separated from the other two. The energies E_R and widths Γ_R of the resonance states are shown in Fig. 2 for varying total coupling strength to the con-

tinuum.

We see the following result. In each group of states there are formed some broad states at high level density. These states do *not* overlap regions outside the interval studied. With further increasing coupling strength, these broad states attract one another in energy and their widths bifurcate. Finally, there are only four broad states according to the four channels. In the separation point, their widths are smaller than the energy region covered by the long-lived states. The question whether there are states lying outside the extension of the spectrum is of interest only when studying the behavior of the short-lived states at a further increased strength of the coupling to the continuum. The resonance trapping in every group is left unchanged by the effects at the borders of the spectrum.

We conclude this section by stating the following. In the random matrix theory, the widths of the trapped resonance states *decrease* as a function of increasing coupling strength κ^{tot}.

III. CONTINUUM SHELL MODEL (CSM) FOR AN OPEN MANY-BODY QUANTUM SYSTEM

In many-body quantum systems, the widths of the long-lived resonance states do not decrease but *saturate* as a function of the coupling strength κ^{tot} [29,30]. In order to investigate the mechanism of saturation we have, according to the results shown in Sec. II B, to go beyond the random matrix theory. In the following, we sketch a model which allows us to describe open *many-body* quantum systems.

The time-independent Schrödinger equation

$$(H-E)|\Psi\rangle=0 \tag{10}$$

is solved in a Hilbert space consisting not only of the discrete many-particle states of a closed system but also of the continuum of decay channels. The potential is assumed to be a spherical one. The Hamilton operator of the system is

$$H=H^0+\hat{V}. \tag{11}$$

H^0 is the unperturbed Hamilton operator describing particles in a finite depth potential and $\hat{V}$ is the operator of the two-body residual interaction between the particles. For details see [9]. The relation between V, Eq. (1), and the two-body operator $\hat{V}$ is considered in [36].

In order to find the solution $|\Psi\rangle$ of Eq. (10) we first solve the shell model problem

$$(E_R^{\mathrm{SM}}-H_{QQ})|\phi_R^{\mathrm{SM}}\rangle=0 \tag{12}$$

in the Q subspace of N discrete states and the coupled channel equations

$$(E^{(+)}-H_{PP})|\xi_E^{c(+)}\rangle=0, \tag{13}$$

with the proper boundary conditions in the P subspace of K coupled channels. The projection operators are $\hat{Q}=\sum_{R=1}^{N}|\phi_R^{\mathrm{SM}}\rangle\langle\phi_R^{\mathrm{SM}}|$ and $\hat{P}=\sum_{c=1}^{K}\int dE|\xi_E^c\rangle\langle\xi_E^c|$. Here $H_{QQ}\equiv\hat{Q}H\hat{Q}$ and $H_{PP}\equiv\hat{P}H\hat{P}$. Further, we solve the coupled channel equations with source term

$$(E^{(+)}-H_{PP})|\omega_R^{(+)}\rangle=\hat{V}_{PQ}|\phi_R^{\mathrm{SM}}\rangle, \tag{14}$$

which connects the two subspaces. Using $\hat{P}+\hat{Q}=1$ we then express $|\Psi\rangle$ by means of the solutions of Eqs. (12)–(14). Care must be taken in order to avoid double counting from Eqs. (12) and (13), i.e., appearance of any resonances in Eq. (13). For this purpose a cutoff technique for single-particle resonances is used in [9] when solving Eq. (13).

In P subspace, the propagator is $G_P^{(+)}=\hat{P}(E+i\epsilon-H_{PP})^{-1}\hat{P}$. The propagator $\hat{Q}(E-H_{QQ}^{\mathrm{eff}})^{-1}\hat{Q}$ in Q subspace contains the effective Hamilton operator in this subspace,

$$H_{QQ}^{\mathrm{eff}}(E)=H_{QQ}+\hat{V}_{QP}G_P^{(+)}\hat{V}_{PQ}. \tag{15}$$

$H_{QQ}^{\mathrm{eff}}(E)$ is non-Hermitian and energy dependent. It has energy-dependent complex eigenvalues $\tilde{\varepsilon}_r=\tilde{E}_R-(i/2)\tilde{\Gamma}_R$ and eigenfunctions $|\tilde{\Phi}_R\rangle$ describing the quasibound states embedded in the continuum (QBSEC) [9]. The $|\tilde{\Phi}_R\rangle$ form a biorthogonal set at each energy E with the orthogonality relation $\tilde{\Phi}_{R'}\rangle=\delta_{RR'}$ (see [21]). Further, it holds that $\langle\tilde{\Phi}_R|\tilde{\Phi}_R\rangle\geq 1$, $\langle\tilde{\Phi}_R|\tilde{\Phi}_{R'}\rangle\in C$ $(R\neq R')$.

Diagonalizing H_{QQ}^{eff} we get the solution of Eq. (10) as

$$|\Psi_E^{(+)}\rangle=|\xi_E^{c(+)}\rangle+\sum_{R=1}^{N}|\tilde{\Omega}_R^{(+)}\rangle\frac{1}{E-\tilde{\varepsilon}_R}\langle\tilde{\Phi}_R|\hat{V}|\xi_E^{c(+)}\rangle. \tag{16}$$

Here the

$$|\tilde{\Omega}_R^{(+)}\rangle=(1+G_P^{(+)}\hat{V})|\tilde{\Phi}_R\rangle \tag{17}$$

are the wave functions of the resonance states R. It should be stressed here once more that $\hat{V}$ is the operator of the *two-body* residual interaction and that the $\tilde{\Phi}_R$ are *many-particle* wave functions.

The relation (17) between the wave functions $\tilde{\Omega}_R^{(+)}$ of the resonance states and the eigenfunctions $\tilde{\Phi}_R$ of H_{QQ}^{eff} is analogous to the Lippman-Schwinger equation

$$|\xi_E^c\rangle=(1+G_P^{(+)}\hat{V})|\chi_E^c\rangle \tag{18}$$

between channel wave functions χ_E^c and coupled channel wave functions ξ_E^c. Therefore $\langle\tilde{\Omega}_R|\hat{V}|\chi_E^{c(+)}\rangle=\langle\tilde{\Phi}_R|\hat{V}|\xi_E^{c(+)}\rangle$. We define the amplitude of the partial width by

$$\tilde{\gamma}_{Rc}\equiv\frac{1}{\sqrt{2\pi}}\langle\tilde{\Omega}_R|\hat{V}|\chi_E^{c(+)}\rangle=\frac{1}{\sqrt{2\pi}}\langle\tilde{\Phi}_R|\hat{V}|\xi_E^{c(+)}\rangle. \tag{19}$$

By inserting the expression (16) for Ψ into the S matrix and using Eq. (19) we get

$$S_{cc'}=e^{2i\delta_c}\delta_{cc'}-2i\pi\langle\chi_E^{c'(-)}|\hat{V}|\xi_E^{c(+)}\rangle+i\sum_R\frac{\tilde{\gamma}_{Rc}\tilde{\gamma}_{Rc'}}{E-\tilde{E}_R+(i/2)\tilde{\Gamma}_R}. \tag{20}$$

The first two terms in Eq. (20) describe the direct reaction part of the process. The last term describes the resonance part, i.e., excitation and deexcitation of the resonance states R. The resonance part $S^{\rm res}_{cc'}$ of the S matrix has the standard Breit-Wigner form. Note, however, that $\widetilde{\gamma}_{Rc}$ is complex and energy dependent. Also $\widetilde{E}_R$ and $\widetilde{\Gamma}_R$ are energy-dependent functions. $S^{\rm res}_{cc'}(E)$ contains the contributions of all the resonance states at the energy E of the system. These contributions may be very different from those at other energies (see [19]).

The poles of the S matrix give the energies E_R and widths Γ_R of the resonance states. They are defined by the fixed-point equations $E_R=\widetilde{E}_R(E=E_R)$ and $\Gamma_R=\widetilde{\Gamma}_R(E=E_R)$. The number of resonance states is exactly equal to the number N of discrete states obtained from Eq. (12) if double counting in P and Q is avoided.

If the energy dependence of $\widetilde{E}_R(E)$ and $\widetilde{\Gamma}_R(E)$ is weak in the interval studied, it holds that $E_R\approx\widetilde{E}_R(E')$ and $\Gamma_R\approx\widetilde{\Gamma}_R(E')$ where E' is an energy somewhere in the middle of the interval. Only under such conditions, E_R and Γ_R can be considered as resonance parameters. Otherwise, the spectroscopic studies performed at the energy E' are meaningful only at this energy since only here are the orthogonality relations between the right and left wave functions fulfilled. The present calculations are performed at the energy $E=E'$ of the system.

According to [21], the decay rates can be defined by $k^{\rm eff}(t)=-(d/dt)\ln\langle\phi(t)|\phi(t)\rangle$ where $\phi(t)$ is the wave function of the system. Using the ansatz $|\phi(t)\rangle=\Sigma_R a_R(t)|\widetilde{\Phi}_R\rangle$ and solving the time-dependent Schrödinger equation with the effective Hamiltonian $H^{\rm eff}_{QQ}$ we get

$$|\phi(t)\rangle=\sum_R a_R(0)e^{-(i/\hbar)[\widetilde{E}_R-(i/2)\widetilde{\Gamma}_R]t}|\widetilde{\Phi}_R\rangle. \tag{21}$$

The $a_R(0)$ define the wave function $\phi(0)$ of the system at the time $t=0$. Neglecting the oscillations caused by the biorthogonality of the function system we get

$$k^{\rm eff}_{\rm gr}(t)=\frac{1}{\hbar}\frac{\Sigma_R A^2_R(t)\widetilde{\Gamma}_R}{\Sigma_R A^2_R(t)}\equiv\frac{1}{\hbar}\,\overline{\Gamma}^{(A)} \tag{22}$$

for the gross time behavior of $k^{\rm eff}$. This is in analogy to $k^{\rm eff}_R=\widetilde{\Gamma}_R/\hbar$ for isolated resonances. The $A^2_R(t)$ are given by $A^2_R(t)=|a_R(0)|^2e^{-\widetilde{\Gamma}_R t/\hbar}\langle\widetilde{\Phi}_R|\widetilde{\Phi}_R\rangle$. They decrease exponentially with the rate $\widetilde{\Gamma}_R/\hbar$. Therefore the $A^2_R(t)$ for the short-lived states are negligible in the long-time scale and the sum in Eq. (22) runs only over the trapped states. If the width distribution of the $N-K$ trapped states is narrow, it holds $\overline{\Gamma}^{(A)}\approx\overline{\Gamma}_{N-K}$. The weighted width $\overline{\Gamma}^{(A)}$ is generally time dependent.

Let us write Eq. (15) more explicitly,

$$H^{\rm eff}_{QQ}(E)=H_{QQ}+\mathcal{P}(E)-iW(E). \tag{23}$$

Here

$$W_{RR'}(E)=\pi\sum_c V^c_R(E)V^c_{R'}(E), \tag{24}$$

where $V^c_R(E)=\langle\phi^{\rm SM}_R|\hat{V}|\chi^{c(+)}_E\rangle$ are real numbers describing the coupling of the shell model states R to the channels c at the energy E of the system and c runs over all open channels. Further,

$$\mathcal{P}_{RR'}(E)=\sum_c {\rm P}\int_{\epsilon_c}^{\infty}V^c_R(E')\,\frac{1}{E-E'}\,V^c_{R'}(E')dE'. \tag{25}$$

P denotes the principal value of the integral and ϵ_c is the threshold energy for the channel c. As a rule, the ϵ_c are different for different channels.

Characteristics of the Hamiltonian of an open many-body quantum system are therefore (i) the different channels are coupled with different strength and (ii) the coupling via the continuum contains not only an imaginary part but also a real part. In the following sections we study the widths of trapped resonance states as a function of increasing coupling strength $\kappa^{\rm tot}$ by considering these properties of the Hamiltonian.

IV. INFLUENCE OF ADDITIONAL WEAKLY COUPLED CHANNELS

In a many-body quantum system, each channel has a certain coupling strength which may be quite different from the coupling strength of other channels. Sources for the different coupling strengths of the channels are, above all, the structure of the states of the residual system, the different angular momenta, and the different threshold energies ϵ_c, see Sec. III.

We study the influence of different coupling strengths of the channels on the resonance trapping in a schematic manner. The main emphasis lies on the question of whether the mean width of the trapped states at strong coupling to the continuum saturates or approaches zero. The study is performed in the random matrix model (RMM) with the Hamiltonian (1) and $N=300$, $K=4$, but different average coupling strength V^2_c to the channels. The ratios among the coupling strengths are $V^2_c/V^2_{c=1}=1$, 0.1, 0.01, and 0.001 [Fig. 3(a)] and $V^2_c/V^2_{c=1}=1$, 0.01, 0.0032, and 0.001 [Fig. 3(b)]. We show κ^j for $j=0,\ldots,5$ averaged over 20 calculations.

The separation points are defined by $\tau_c=1$ for any channel, i.e., $x_c=1$ for a certain c [see Eqs. (3) and (5)]. These points are given by $\kappa^{\rm tot}=\Sigma^K_{c'=1}V^2_{c'}/V^2_c$. This gives $\kappa^{\rm tot}=1.11$, 11.1, 111, 1110 in Fig. 3(a) and $\kappa^{\rm tot}=1.01$, 101, 321, 1010 in Fig. 3(b).

In Fig. 3(a) there is at $\kappa^{\rm tot}\approx1.2$ a separation point, where one broad state separates from the other ones and the mean width of the remaining resonance states starts to decrease. Here, κ^j for $j>0$ decreases slightly, but soon increases again under the influence of the next channel. At $\kappa^{\rm tot}\approx12$ a second broad state separates from the other ones. Similar situations occur at $\kappa^{\rm tot}\approx120$ and $\kappa^{\rm tot}\approx1200$. Finally there are four broad states corresponding to the four channels. For still larger values of $\kappa^{\rm tot}$, the values κ^j, $j>3$ decrease. Note that the values κ^j, $j>4$ are almost constant in the region $1<\kappa^{\rm tot}<1500$. Thus different coupling strengths to the chan-

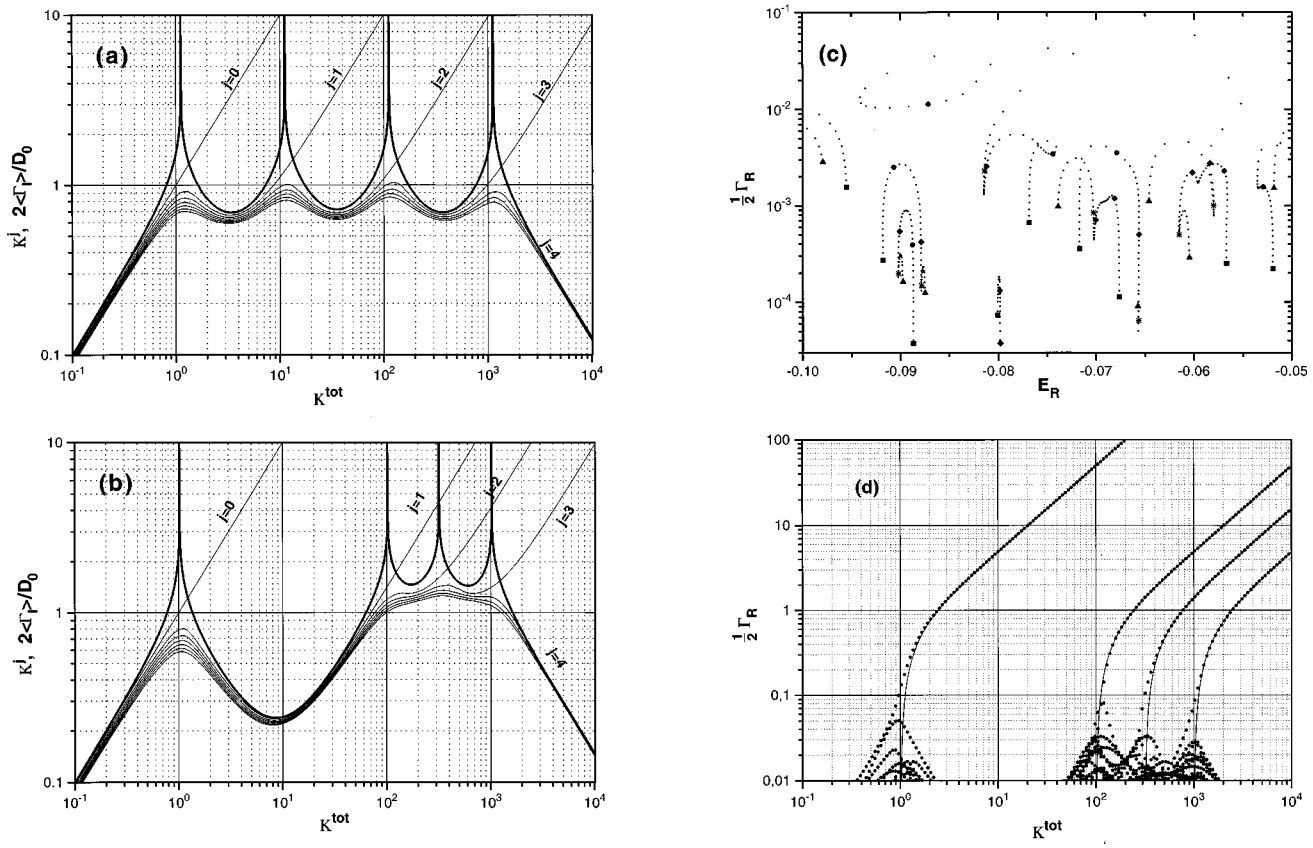

FIG. 3. κ^j for $j=0,\ldots,6$ versus κ^{tot} in the RMM for $N=300$ and $K=4$ with the ratios of the coupling strengths $V_c^2/V_{c=1}^2=1$, 0.1, 0.01, 0.001 (a) and $V_c^2/V_{c=1}^2=1$, 0.01, 0.0032, 0.001 (b). Eigenvalue picture (c) and $\frac{1}{2}\Gamma_R$ (dots) together with the function $\frac{1}{2}(x_c-1/x_c)$, Eq. (7), (full line) versus κ^{tot} (d) for $V_c^2/V_{c=1}^2=1$, 0.01, 0.0032, and 0.001. In (a) and (b), $2\langle\Gamma_l\rangle/D_0$ versus κ^{tot} is shown with a thick line. In (c), the points for $\kappa^{\mathrm{tot}}=0.1$, 1, 10, 100, and 1000 are marked with triangles, stars, diamonds, large dots, and squares, respectively.

nels are a source for saturation of the average width of the long-lived $N-K$ states as a function of κ^{tot}.

In Fig. 3(b) we have one strongly coupled channel and a group of weakly coupled ones. At $\kappa^{\mathrm{tot}}\approx 1.1$ a picture similar to ordinary trapping with one channel can be seen. One state separates and the widths of the remaining ones decrease. For larger coupling to the continuum, however, the widths of the trapped states start to increase under the influence of the weakly coupled channels. A new critical region occurs between $\kappa^{\mathrm{tot}}\approx 70$ and 2000 where three states corresponding to the three new channels separate. In this region, the widths of the trapped states saturate and thereafter their widths decrease.

Further, these two examples show another interesting result. At the points where a broad state separates from the remaining ones, we have $\tau_c\approx 1$ for a certain channel c, see the thick line ($2\langle\Gamma_l\rangle/D_0$ versus κ^{tot}). When all $\tau_c<1$, we have good agreement between the $\langle\Gamma_l\rangle$ calculated from Eqs. (3) and (4) and the calculated mean width $\overline{\Gamma}_{N-j}$. Here, j is determined by the number of broad states and $j=0$ only for $\kappa^{\mathrm{tot}}<1$ (compare Sec. II B).

A small part of the eigenvalue picture (E_R and Γ_R), Fig. 3(c) [$V_c^2/V_{c=1}^2=1$, 0.01, 0.0032, and 0.001 as in Fig. 3(b), but only one calculation], shows width increase, energy shift, width decrease, and once again increase, shift, and decrease. The renewed increase of the widths of the states trapped by the first channel is caused by the fact that the new channels become active only at strong coupling to the continuum.

In Fig. 3(d) we show $\Gamma_R/2$ and $(x_c-1/x_c)/2$, $c=1,\ldots,4$, Eq. (7), versus κ^{tot} for the same calculation as in Fig. 3(c). The agreement between (x_c-1/x_c) and the four different widths Γ_s of the short-lived states illustrates nicely that the separation of every broad mode takes place from the group of long-lived resonance states. This means the separation process is more or less independent of the broad modes separated at smaller values of κ^{tot}.

V. THE ROLE OF THE REAL PART OF THE COUPLING TERM

A. Two resonances coupled to one common channel

The influence of a real part on the phenomenon of resonance trapping can be seen by means of the following simple model for two resonance states coupled to one common decay channel,

$$h^{\mathrm{eff}}=\begin{pmatrix}1 & 0\\ 0 & -1\end{pmatrix}-2i\alpha e^{-i\theta}\begin{pmatrix}\cos^2\varphi & \cos\varphi\sin\varphi\\ \cos\varphi\sin\varphi & \sin^2\varphi\end{pmatrix},$$
$$-90^\circ\leqslant\theta\leqslant 90^\circ. \tag{26}$$

Here the relative coupling strength of the two states to the continuum may be varied by means of the angle φ ($\varphi\neq 0^\circ,90^\circ,\ldots$). The angle θ determines the ratio between the real and imaginary part of the coupling term. In [16] the case $\theta=0$ has been studied.

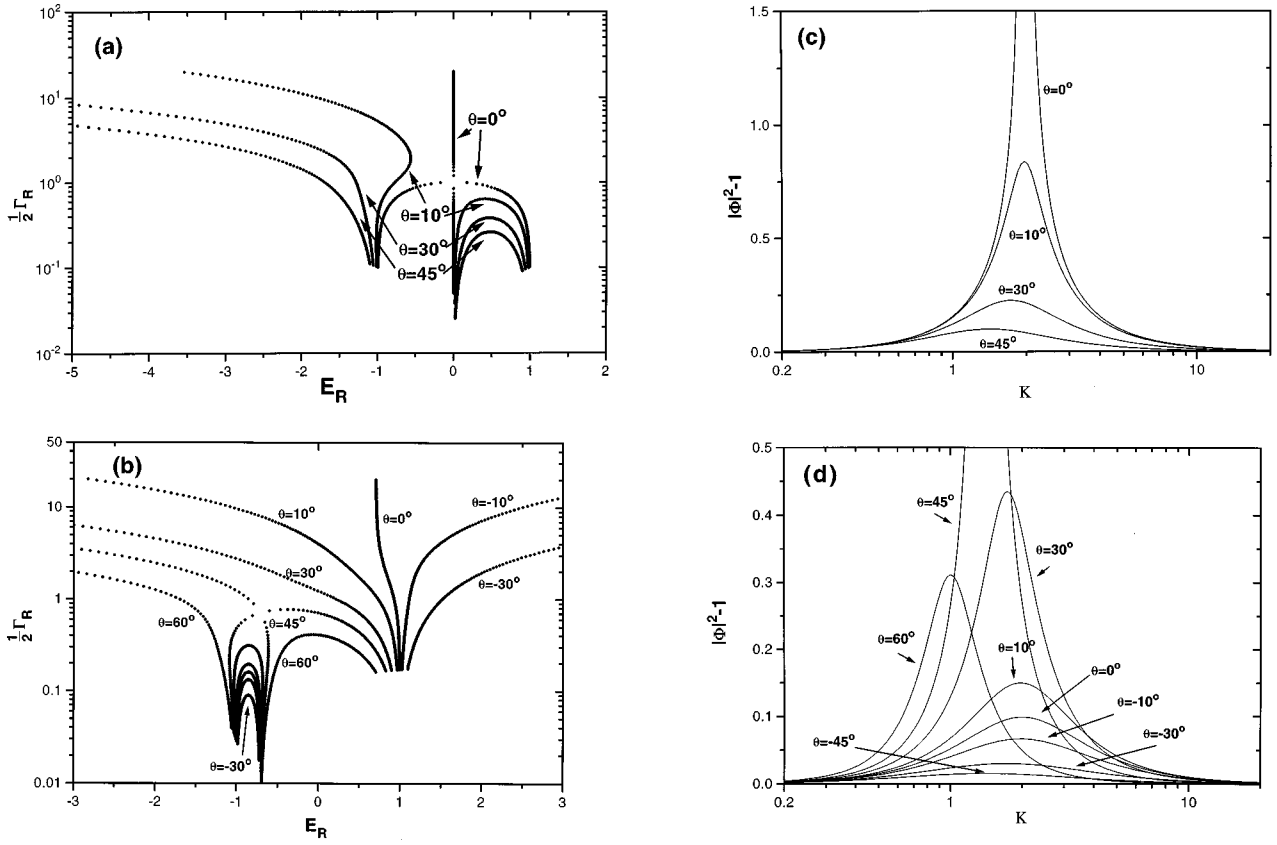

FIG. 4. Eigenvalue picture ($\frac{1}{2}\Gamma_R$ and E_R) calculated for different κ [(a), (b)] and $|\Phi|^2$ versus κ [(c), (d)] for two states coupled to one channel. It is $\varphi=45°$ [(a), (c)] and $\varphi=22.5°$ [(b), (d)]. The values are shown for some different θ in the same plots (see the text for details). Note the logarithmic scales.

The eigenvalues of h^{eff} are

$$\varepsilon_{\pm}=-i\alpha e^{-i\theta}\pm\sqrt{1-2i\alpha e^{-i\theta}\cos(2\varphi)-\alpha^2e^{-2i\theta}}. \tag{27}$$

At $\alpha=0$ we have two states lying at the energies -1 and 1. Their widths increase with increasing α up to some critical value $\alpha_{\text{crit}}\leqslant 1$. The eigenvectors of h^{eff} are

$$\Phi_{\pm}=\frac{1}{\sqrt{-\alpha^2e^{-2i\theta}\sin^2(2\varphi)+\phi_{\pm}^2}}\begin{pmatrix} i\alpha e^{-i\theta}\sin(2\varphi)\\ \phi_{\pm}\end{pmatrix}. \tag{28}$$

Here, the normalization of the wave functions is made according to $\langle\Phi_{\pm}^{*}|\Phi_{\pm}\rangle=1$ and $\phi_{\pm}=1-2i\alpha e^{-i\theta}\cos^2(\varphi)-\varepsilon_{\pm}$. In our case of only two resonance states, the values $|\Phi_{\pm}|^2$ are the same for both states.

The distance in the complex plane between the two eigenvalues is

$$|\varepsilon_{+}-\varepsilon_{-}|=2|\sqrt{1-2i\alpha e^{-i\theta}\cos(2\varphi)-\alpha^2e^{-2i\theta}}|\equiv 2|S|. \tag{29}$$

Using S, the denominator in Eq. (28) can be rewritten as

$$\sqrt{-\alpha^2e^{-2i\theta}\sin^2(2\varphi)+\phi_{\pm}^2}=\sqrt{2S\{S\mp[1-ie^{-i\theta}\cos(2\varphi)]\}}. \tag{30}$$

The factor $S\pm[1-ie^{-i\theta}\cos(2\varphi)]$ is never zero (for $\theta\neq\pm\pi/2$), and thus $|\Phi|^2\to\infty$ if and only if the distance in the complex plane between the two eigenvalues goes to zero.

Let us define $\kappa=(\Gamma_1+\Gamma_2)/L$ where $L=2$ is the distance between the two resonance states. For the Hamiltonian (26) it holds that $\kappa=2\alpha\cos\theta$.

In the following the two cases $\varphi=22.5°$ and $\varphi=45°$ are studied in detail. In the first case both states are coupled with equal strength to the decay channel while in the second case the state having the initial energy $+1$ is more strongly coupled to the channel than the other one.

In Fig. 4 the complex eigenvalues [4(a)] and the $|\Phi|^2$ versus κ [4(c)] are shown for $\varphi=45°$ and $\theta=0°$, 10°, 30°, and 45°. The different points in Fig. 4(a) correspond to different values of κ, $0.2\leqslant\kappa\leqslant 20$. As κ grows, each eigenvalue follows a certain trajectory. For $\theta=0°$ the E_R and Γ_R of the two states meet in one point in the complex plane at $\kappa=\kappa_{\text{crit}}=2$. Here $|\Phi(\kappa_{\text{crit}})|^2\to\infty$. Beyond this separation point, one state continues to increase in width whereas the width of the other one decreases (*resonance trapping*). For $\theta>0$ the state with initial energy -1 becomes the broader one and is shifted towards negative energies. In contrast to this, for all $\theta<0$ (not shown in the figures) the state with initial energy $+1$ becomes, in this symmetrical case $\varphi=45°$, the broader one and is shifted towards large positive energies. For $\theta\neq 0°$ the minimum distance in the complex plane between the two states remains different from zero and $|\Phi|^2$ remains finite for all κ with its maximum value at κ_{crit}. As $\theta\to 90°$, h^{eff} becomes Hermitian. In this limit, $|\Phi|^2\to 1$ and $\kappa_{\text{crit}}\to 0$.

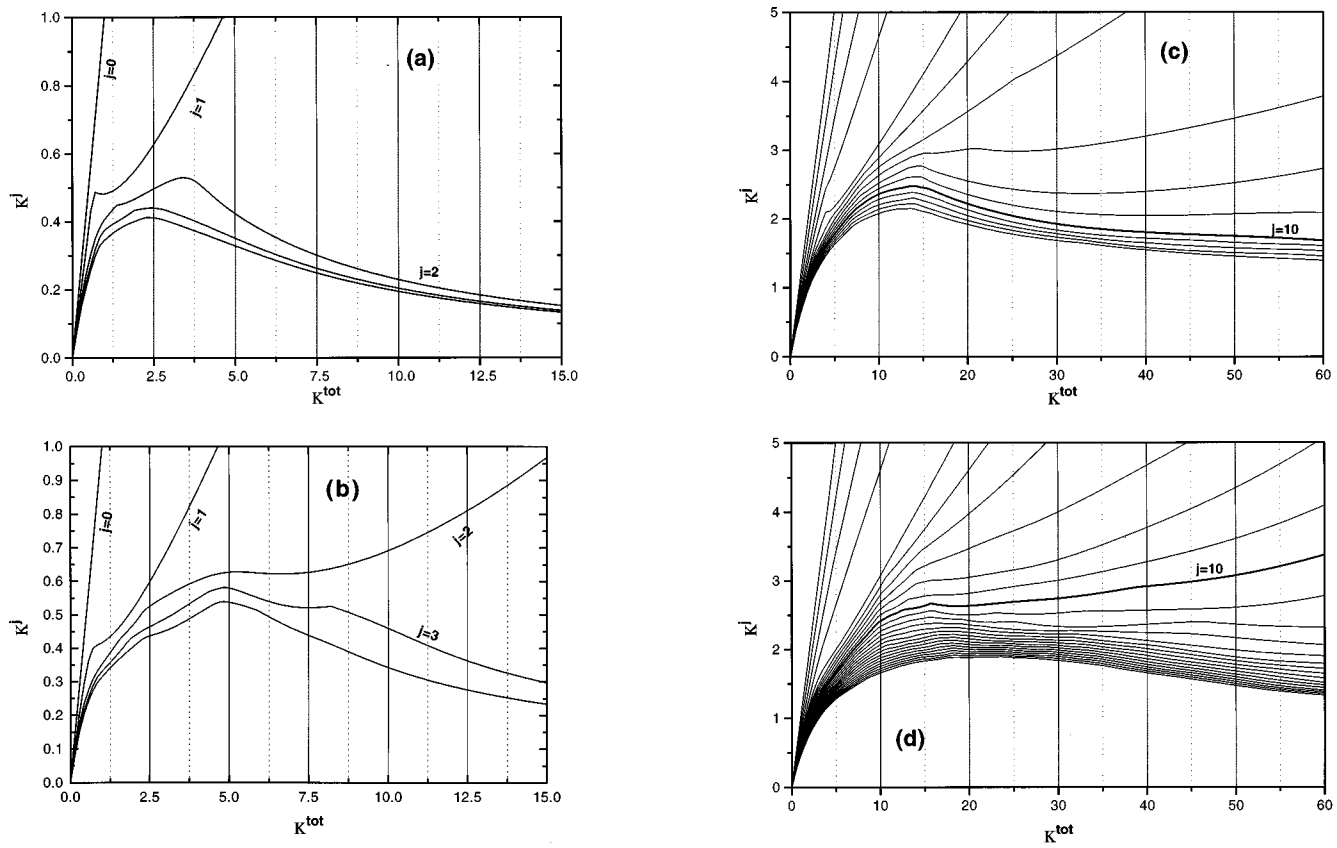

FIG. 5. κ^j versus κ^{tot} in the CSM for 190 resonance states in ^{16}O with $J^\pi=1^-$, $K=2$ [(a), (b)] and $K=10$ [(c), (d)] channels. In [(a), (c)] $\mathcal{P}=0$ while $\mathcal{P}$ is taken into account in [(b), (d)]. It is $j=0,\ldots,4$ [(a), (b)], $j=0,\ldots,14$ (c) and $j=0,\ldots,25$ (d). The calculations are performed at $E=29$ MeV.

The case $\varphi=22.5°$ is shown in Figs. 4(b) (complex eigenvalues) and 4(d) ($|\Phi|^2$ versus κ) for some values of θ ranging from $-45°$ to $+60°$. For $\theta>0$ the state with initial energy $E_R=+1$, being the broader one at small κ, gets an extra shift towards small energies whereas the shift is towards large energies for $\theta<0$. κ_{crit} is a function of only $|\theta|$ and has the same values as in the symmetrical case. It has its largest value for $\theta=0°$. At $\theta=45°$ the complex eigenvalues of the two states meet in one point and $|\Phi(\kappa_{\mathrm{crit}})|^2$ diverges. As $\theta\rightarrow\pm 90°$ h^{eff} becomes Hermitian and $|\Phi(\kappa^{\mathrm{crit}})|^2\rightarrow 1$. For $-90°<\theta<45°$ the state with initial energy $E_R=-1$ is the one becoming trapped. For $45°<\theta<90°$, however, the state with initial energy $E_R=+1$ becomes trapped even though that state is the broader one at small κ.

These examples show that the details of the resonance trapping change when allowing for extra energy shifts by introducing the angle θ in Eq. (26). They are basic for an understanding of the results of the following sections.

B. *N* resonance states coupled to *K* common channels

We study the influence of the real part of the coupling term on the mean width of the trapped states in the framework of the CSM. We do this by comparing the results of calculations with and without $\mathcal{P}$, Eq. (23), taken into account.

The rank of $\mathcal{P}$ is, generally, larger than K. $\mathcal{P}$ increases with α by approximatively the same factor as W. Thus the Hermitian part $H_{QQ}+\mathcal{P}$ of H^{eff}_{QQ} is never a small perturbation on W and the rank of H^{eff}_{QQ} is larger than K also in the strong coupling limit (compare Sec. II B). Nevertheless, resonance trapping occurs also when taking $\mathcal{P}$ into account.

In Fig. 5 we present κ^j versus κ^{tot} for some calculations in the CSM. As in the RMM, we use $D_0=L/(N-1)$ where L is the length of the spectrum of H_{QQ}. We study 190 resonance states in ^{16}O with $J^\pi=1^-$ and vary α. In the first case [Figs. 5(a) and 5(b)] we study the reaction $^{15}\mathrm{O}_{1/2^-}(n,n)^{15}\mathrm{O}_{1/2^-}$ giving $K=2$ channels with s and d waves, respectively. The second case [Figs. 5(c), 5(d)] is $^{15}\mathrm{N}_{1/2^-}(p,x)Y$ where $x=p$, n and $Y=^{15}\mathrm{N}_{1/2^-,3/2^-}$, $^{15}\mathrm{O}_{1/2^-,3/2^-}$ which gives $K=10$ channels. Figures 5(a), 5(c) and 5(b), 5(d) are without and with $\mathcal{P}$, respectively.

Figures 5(a) and 5(c) with $\mathcal{P}=0$ are similar to Figs. 3(a) and 3(b). In Fig. 5(a) we have two channels with different coupling strength. First we see the increase of the mean width of all the states for small coupling to the continuum up to the separation point corresponding to the strong channel. Thereafter we have a region of saturation of the mean width and the separation point for the second broad state. In Fig. 5(c) we see first the separation of four strongly coupled states and the saturation of the widths up to the coupling strength at which ten states corresponding to the ten channels are separated from the remaining ones. Finally the mean width of all the trapped states decreases.

In the calculations with the principal value integral $\mathcal{P}$ taken into account, we additionally see another effect [Figs.

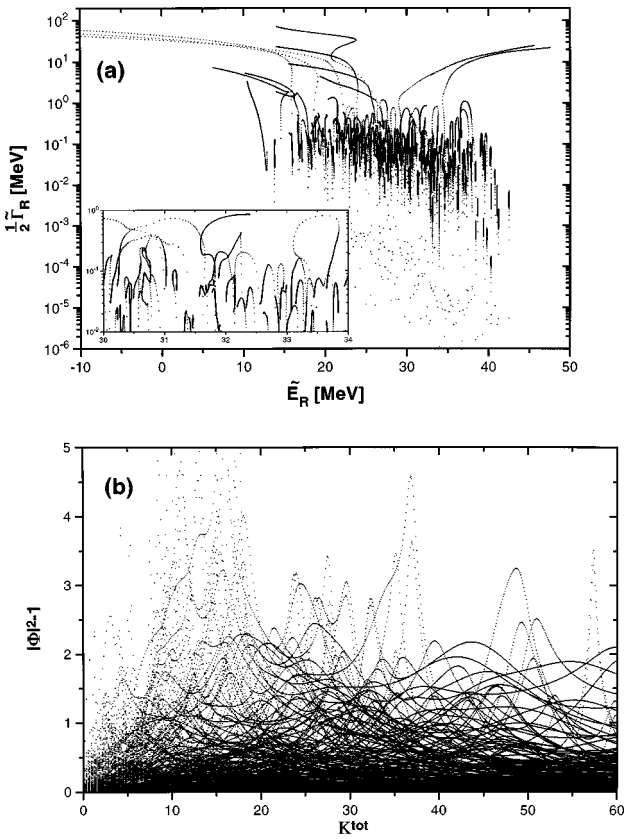

FIG. 6. Eigenvalue picture ($\frac{1}{2}\tilde{\Gamma}_R$ and $\tilde{E}_R$) for different coupling strengths $0.008 \leqslant \kappa^{\mathrm{tot}} \leqslant 60$ (a) and $|\tilde{\Phi}_R|^2$ versus κ^{tot} (b) in the CSM. $N=190$ resonance states in ^{16}O with $J^{\pi}=1^-$ and $K=10$. $\mathcal{P}$ is taken into account [compare Fig. 5(d)].

5(b) and 5(d)]. There are, at strong coupling to the continuum, not only K broad states, but more states separate from the remaining ones and get large widths. In Fig. 5(d) we have at $\kappa^{\mathrm{tot}}=60$ about 15 states that are broad but the sharp distinction between the lifetimes of the broad and the trapped states is washed out.

Similar results are obtained by studying other resonance states with other quantum numbers.

In the eigenvalue picture, Fig. 6(a), we show $\tilde{E}_R$ and $\tilde{\Gamma}_R$ for the same resonance states as in Fig. 5(d) by varying κ^{tot} in the interval $0.008 \leqslant \kappa^{\mathrm{tot}} \leqslant 60$. Note that the steps in κ^{tot} are approximatively equidistant. We see extra shifts in energy caused by the principal value integral $\mathcal{P}$. Such a shift is, generally, in the order of magnitude of the width of the state, i.e., it is large for states getting large widths with increasing coupling strength to the continuum. That means the broad states leave the energy region where the trapped states are lying. These shifts are similar to those in Figs. 4(a) and 4(b) for $\theta \neq 0$.

Figure 6(a) illustrates also the behavior of trapped states under the influence of increasing coupling to the continuum. First their widths increase, then the states get trapped, i.e., their widths start to decrease and they get a small energy shift. For even stronger coupling to the continuum the widths can start to increase again with a renewed energy shift and so on. In distinction to Figs. 1(b) and 3(c), these shifts have mainly two origins: the energy attraction accompanying the bifurcation of the widths *and* the influence of $\mathcal{P}$.

The corresponding $|\tilde{\Phi}_R|^2$ as a function of κ^{tot} are shown in Fig. 6(b). The $|\tilde{\Phi}_R|^2$ remain larger than 1 also at large values of κ^{tot}. This indicates further avoided resonance crossings which cause, ultimately, the saturation of the widths of the long-lived resonance states.

Summarizing, the $\mathcal{P}$ enlarges the critical region of reorganization where the local process of resonance trapping takes place. The mean width of the long-lived states saturates but there is no longer a sharp distinction between the broad states and the long-lived ones.

VI. RESONANCE TRAPPING AND BROADENING OF THE WIDTH DISTRIBUTION

In the RMM with equally strongly coupled channels it is shown in, e.g., [26,22] that the width distribution in the critical region of reorganization is broader than in noncritical regions. In noncritical regions, i.e., as long as all transmission coefficients are small, the width distribution follows a χ^2_K law with the number of degrees of freedom corresponding to the number K of open channels [8]. In this section we study the width distribution in the RMM with varying coupling strengths to the channels and in the CSM.

In the RMM with varying coupling strengths of the channels we have tried to fit the width distribution in noncritical regions to a χ^2_K distribution. The error in the fit is large even for small transmission coefficients. We conclude that the system must be coupled to all the channels with comparable strengths for the widths to be χ^2_K distributed.

In the following we therefore study the broadening of the width distribution by calculating the normalized variance σ_y^j of the widths,

$$\sigma_y^j = \sqrt{\frac{1}{N-j}\sum_{R=1}^{N-j}(y_R-1)^2}, \quad y_R=\Gamma_R/\overline{\Gamma}_{n-j} \qquad (31)$$

where the sum runs over all but the j broadest states. The theoretical value obtained in the RMM with K equally strongly coupled channels for the (trapped) states far from the critical region of reorganization is $\sigma_y^{j=K}=\sqrt{2/K} \equiv \sigma_y^{\mathrm{RMM}}$.

The results of calculations in the RMM with varying coupling strengths to the channels are shown in Fig. 7. In Fig. 7(a) σ_y^j is shown for $K=10$ channels with $V_c^2/V_{c=1}^2$ distributed on [1,...,0.1] with equal distances at the logarithmic scale for $j=0,\ldots,13$. In Figs. 7(b) and 7(c) we show σ_y^j for $K=4$ channels and $j=1,\ldots,6$ with $V_c^2/V_{c=1}^2=1$, 0.1, 0.001, 0.001 and $V_c^2/V_{c=1}^2=1$, 0.01, 0.0032, 0.001, respectively [compare Figs. 3(a), 3(b)]. Note that σ_y^j before the separation of a broad state should be compared with the value σ_y^{j+1} after the separation.

In the figures, the values $\sigma_y^{\mathrm{RMM}}=\sqrt{2/K}$ are shown with a dashed line. In the case of different coupling strengths of the K channels, the width distribution is broader than in the case of K channels with comparable coupling strengths.

The separation of every broad state is accompanied by a broadening of the width distribution, see Figs. 7(a)–7(c). The distribution between the separation points in Fig. 7(b) and between the separation points of the first and second broad

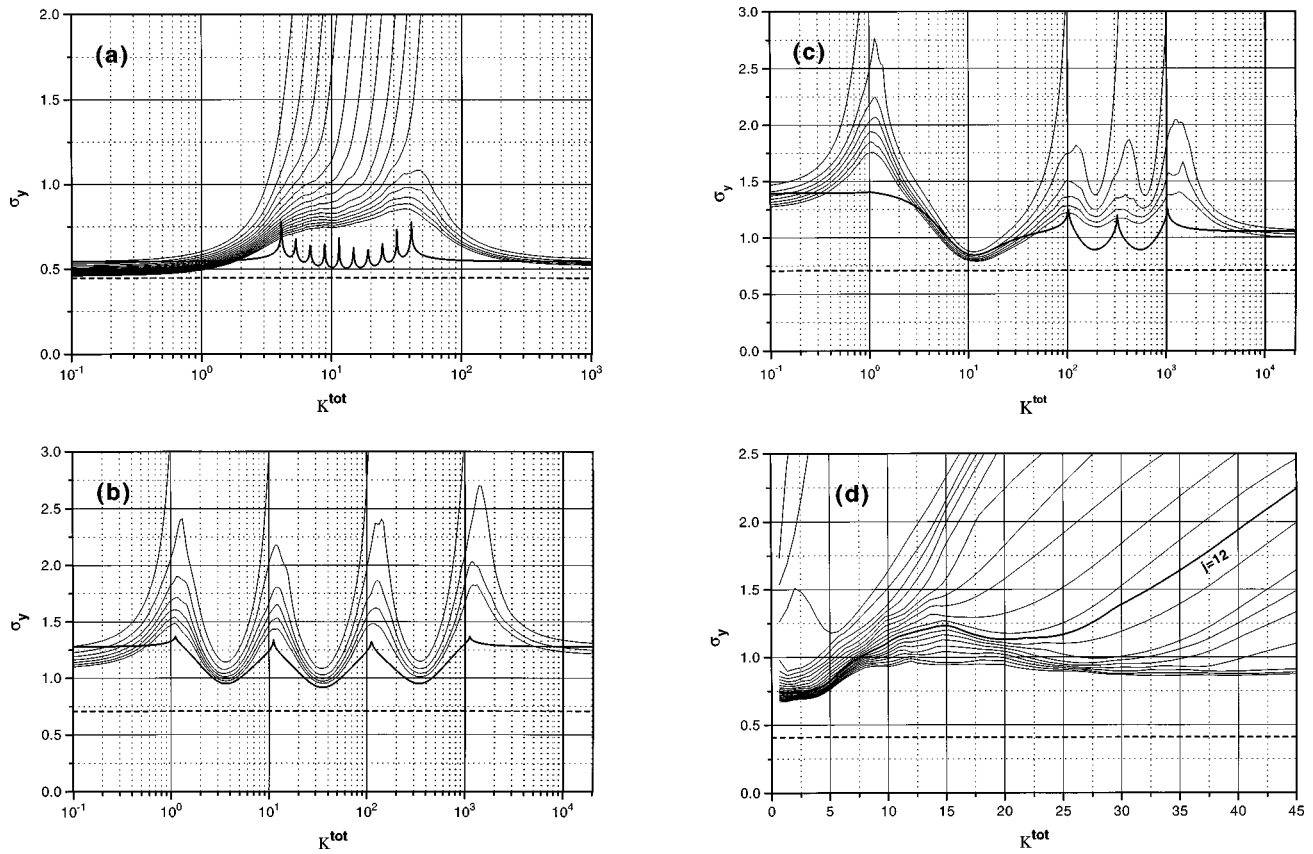

FIG. 7. σ_y^j, σ_y^l, and σ_y^{RMM} versus κ^{tot} in the RMM for three selected values of $V_c^2/V_{c=1}^2$ (for details see the text). σ_y^j is shown for $j=0,\ldots 14$ (a) and $j=0,\ldots,6$ [(b), (c)]. The thick lines are σ_y^l obtained from Eq. (33) and the dashed lines are σ_y^{RMM}. (d) σ_y^j for $j=1,...,20$ versus κ^{tot} in the CSM for $J^\pi=2^-$, $K=12$, and $\mathcal{P}$ is taken into account. $j=0,\ldots,20$ and the dashed line is σ_y^{RMM} for $K=12$.

state in Fig. 7(c) is, however, narrower than the distributions for very small and very large κ^{tot}.

To describe the distribution of the long-lived states in regions where all $\tau_c<1$ we make the following ansatz, compare Eq. (3):

$$\Gamma_R^l=-\frac{d}{2\pi}\sum_c \ln(1-\tau_c)g_{R,c}^2. \tag{32}$$

Here $g_{R,c}^2$ for a certain c is a Gaussian distributed vector with mean zero and variance 1 and τ_c is the transmission coefficient defined in Eq. (5).

The normalized variance of Γ_R^l is

$$\sigma_y^l=\frac{\sqrt{\overline{(\Gamma_R^l)^2}-\overline{(\Gamma_R^l)^2}}}{\overline{\Gamma_R^l}}=\frac{\sqrt{2\Sigma_c[\ln(1-\tau_c)]^2}}{-\Sigma_c\ln(1-\tau_c)}\geqslant\sigma_y^{\mathrm{RMM}}. \tag{33}$$

(Note that $\overline{g^2}=1$ and $\overline{g^4}=3$.) $\sigma_y^l=\sigma_y^{\mathrm{RMM}}$ for the same number K of open decay channels holds only when all τ_c are equal. The values calculated from Eq. (33) are shown with a thick line in Figs. 7(a)–7(c). The variances are well described by Eq. (33) in regions of the coupling strength κ^{tot} with all $\tau_c<1$.

The values σ_y^j as a function of κ calculated in the CSM are similar to those obtained in the RMM. One example is shown in Fig. 7(d) for the case $J^\pi=2^-$ with $K=12$ open channels.

We conclude that in many-body quantum systems, the distribution of the widths is broader than in the RMM with equal coupling strength to the channels (also at small transmission coefficients). This result explains the broadening of the width distribution described in the literature by introducing an effective number K^{eff} of channels being smaller than K.

For the case shown in Fig. 7(a), we have calculated also $k_{\mathrm{gr}}^{\mathrm{eff}}$, Eq. (22), as a function of time t with 12 different coupling strengths κ^{tot} of the system to the channels (Fig. 8). $\hbar=1$. In Table I the values κ^{tot} and $\overline{\Gamma}_{N-K}$ for the different curves are given. All the curves $a-f$, being below the critical region, differ considerably from one another. Inside the critical region, the curves for different κ^{tot} $(g-i)$ are, however, similar to one another.

As a result, weakly coupled channels cause a saturation of the mean value $\overline{\Gamma}_{N-j}$ as a function of κ^{tot}. Since the width distribution σ_y^j does not change much, also $k_{\mathrm{gr}}^{\mathrm{eff}}$ saturates in the long-time scale, i.e., $k_{\mathrm{gr}}^{\mathrm{eff}}$ remains almost unchanged by

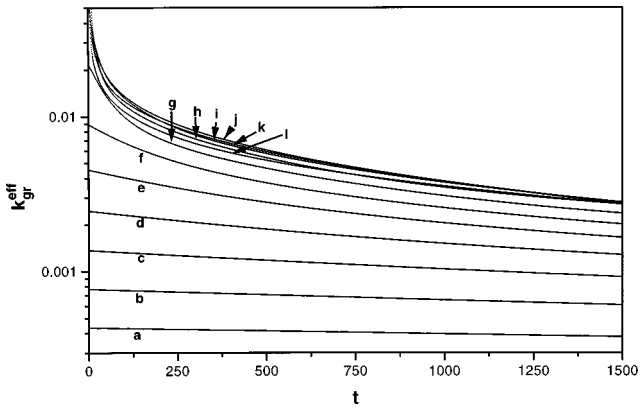

FIG. 8. k_{gr}^{eff} versus time t for $K=10$ and $V_c^2/V_{c=1}^2=1,\ldots,0.1$ [compare Fig. 7(a)]. The 12 curves are calculated with κ^{tot} between 0.1 and 50. κ^{tot} and $\overline{\Gamma}_{N-K}$ for the curves are given in Table I.

varying κ^{tot} in the critical region. The saturation is related to the enlarged width distribution.

VII. CONCLUSION

In this paper we studied the positions and widths of resonance states in a many-body quantum system with N resonance states as a function of increasing coupling strength κ^{tot} to the continuum which consists of $K \ll N$ decay channels. In a critical region of the coupling strength, the system reorganizes itself under the influence of the decay channels. The local process is the avoided crossing of two resonance states which takes place whenever the distance in energy between the states is comparable to the sum of their widths. It is accompanied by an essential biorthogonality of the eigenfunctions of H^{eff}. As a result, one state continues to increase in width whereas the other one decreases with further increasing coupling strength (resonance trapping). For a system with many states, this leads to a broadening of the width distribution.

With further increased coupling strength, the broadening of the width distribution goes over into a separation of time scales if $K \ll N$. The smaller K, the better expressed is this separation. Weakly coupled channels as well as the Hermitian part of the coupling term $\hat{V}_{QP}G_P^{(+)}\hat{V}_{PQ}$ have the tendency of washing out the differences between the lifetimes of the group of long-lived trapped states, on the one hand, and the group of short-lived states, on the other hand.

TABLE I. κ^{tot} and $\overline{\Gamma}_{N-K}$ for the different curves in Fig. 8.

Curve	κ^{tot}	$\overline{\Gamma}_{N-K}$
a	0.10	0.094
b	0.18	0.17
c	0.31	0.29
d	0.54	0.51
e	0.96	0.89
f	1.7	1.5
g	3.0	2.6
h	5.2	3.9
i	9.2	4.7
j	16.	4.9
k	28.	4.5
l	50.	3.3

We studied in detail the widths of the $N-j$ long-lived trapped states under different conditions. We introduced additional channels to which the system is weakly coupled and we took into account the Hermitian part of $\hat{V}_{QP}G_P^{(+)}\hat{V}_{PQ}$ in H_{QQ}^{eff}, Eq. (15). Under the influence of these additional terms in the Hamiltonian, the trapped states can increase their widths and change their positions in energy. Thus trapped resonance states may again come close to each other if the coupling to the continuum is stronger. The resonance crossing is avoided and accompanied by an essential biorthogonality of the eigenfunctions of H^{eff} in the same manner as at smaller coupling strength. As a result of all these processes, the average width of the states saturates as a function of the coupling strength to the continuum when an appropriate number of states with the largest widths is excluded from the mean value. This number is equal to the number of open decay channels as long as the real part of the coupling term $\hat{V}_{QP}G_P^{(+)}\hat{V}_{PQ}$ is small compared to its imaginary part.

The width distribution of the long-lived states is related to the transmission coefficients. If all transmission coefficients are equal and smaller than one, the widths are χ_K^2 distributed where K is the number of channels. In many-body quantum systems with different coupling strengths to the different decay channels, the distribution is broader than a χ_K^2 distribution also for small transmission coefficients.

The decay rates are related to the mean decay widths of the long-lived states. This means the decay rates also saturate in quantum systems at high level density as a function of the coupling strength κ^{tot}.

Summarizing the results we state that resonance trapping is a realistic process occurring in many-particle quantum systems at high level density. It leads to a saturation of both the decay rates and the average decay width of the long-lived states as well as to a broadening of the width distribution and—if the number of open decay channels is not too large—to a separation of time scales. That means the decay rates and the decay widths of the long-lived resonance states show the same behavior not only at low level density but also at high level density. The saturation is caused in both cases by the finite number $K<N$ of channels into which the N resonance states can decay. The application of the standard random matrix approach to the details of the trapping process in an ensemble of resonance states is limited.

We would like to state once more that the time deexcitation of resonance states at high level density should be directly measured. The results could make a proof of the phenomenon of resonance trapping possible.

ACKNOWLEDGMENTS

We gratefully acknowledge valuable discussions with V. A. Mandelshtam, M. Müller, H. Reisler, T. H. Seligman, G. Soff, and H. S. Taylor. This work is supported by DFG (Grant No. Ro 922).

[1] V. V. Sokolov, I. Rotter, D. V. Savin, and M. Müller, Phys. Rev. C **56**, 1031 (1997); **56**, 1044 (1997).
[2] E. P. Kanter, D. Kollewe, K. Komaki, I. Leuca, G. M. Temmer, and W. M. Gibson, Nucl. Phys. A **299**, 230 (1978).
[3] N. E. Karapanagioti, O. Faucher, Y. L. Shao, D. Charalambidis, H. Bachau, and E. Cormier, Phys. Rev. Lett. **74**, 2431 (1995).
[4] P. Kleinwächter and I. Rotter, Phys. Rev. C **32**, 1742 (1985); F. M. Dittes, W. Cassing, and I. Rotter, Z. Phys. A **337**, 243 (1990); R. D. Herzberg, P. von Brentano, and I. Rotter, Nucl. Phys. A **556**, 107 (1993); W. Iskra, M. Müller, and I. Rotter, Phys. Rev. C **51**, 1842 (1995); E. Sobeslavsky, F. M. Dittes, and I. Rotter, J. Phys. A **28**, 2963 (1995).
[5] H. Friedrich and D. Wintgen, Phys. Rev. A **32**, 3231 (1985); A. Bürgers and D. Wintgen, J. Phys. B **27**, L131 (1994).
[6] V. V. Sokolov and V. G. Zelevinsky, Phys. Lett. B **202**, 10 (1988); F. Haake, F. Izrailev, N. Lehmann, D. Saher, and H. J. Sommers, Z. Phys. B **88**, 359 (1992); F. M. Izrailev, D. Saher, and V. V. Sokolov, Phys. Rev. E **49**, 130 (1994).
[7] V. B. Pavlov-Verevkin, Phys. Lett. A **129**, 168 (1988); F. Remacle, M. Munster, V. B. Pavlov-Verevkin, and M. Desouter-Lecomte, *ibid.* **145**, 365 (1990); M. Desouter-Lecomte and V. Jacques, J. Phys. B **28**, 3225 (1995); F. Remacle and R. D. Levine, Phys. Lett. A **211**, 284 (1996); F. Remacle and R. D. Levine, J. Phys. Chem. **100**, 7962 (1996); M. Desouter-Lecomte and J. Liévin, J. Chem. Phys. **107**, 1428 (1997).
[8] V. V. Sokolov and V. G. Zelevinsky, Nucl. Phys. A **504**, 562 (1989).
[9] I. Rotter, Rep. Prog. Phys. **54**, 635 (1991).
[10] F. M. Dittes, I. Rotter, and T. H. Seligman, Phys. Lett. A **158**, 14 (1991).
[11] F. M. Dittes, H. L. Harney, and I. Rotter, Phys. Lett. A **153**, 451 (1991).
[12] V. V. Sokolov and V. G. Zelevinsky, Ann. Phys. (N.Y.) **216**, 323 (1992).
[13] W. Iskra, I. Rotter, and F. M. Dittes, Phys. Rev. C **47**, 1086 (1993).
[14] W. Iskra, M. Müller, and I. Rotter, J. Phys. G **19**, 2045 (1993); **20**, 775 (1994).
[15] K. Someda, H. Nakamura, and F. H. Mies, Chem. Phys. **187**, 195 (1994).
[16] M. Müller, F.-M. Dittes, W. Iskra, and I. Rotter, Phys. Rev. E **52**, 5961 (1995).
[17] M. Desouter-Lecomte, J. Liévin, and V. Brems, J. Chem. Phys. **103**, 4524 (1995).
[18] U. Peskin, W. H. Miller, and H. Reisler, J. Chem. Phys. **102**, 8874 (1995).
[19] E. Persson, M. Müller, and I. Rotter, Phys. Rev. C **53**, 3002 (1996).
[20] S. Drozdz, A. Trellakis, and J. Wambach, Phys. Rev. Lett. **76**, 4891 (1996).
[21] E. Persson, T. Gorin, and I. Rotter, Phys. Rev. E **54**, 3339 (1996).
[22] Y. V. Fyodorov and H. J. Sommers, Pis'ma Zh. Eksp. Teor. Fiz. **63**, 970 (1996) [JETP Lett. **63**, 1026 (1996)].
[23] V. V. Flambaum, A. A. Gribakina, and G. F. Gribakin, Phys. Rev. A **54**, 2066 (1996).
[24] V. A. Mandelshtam and H. S. Taylor, J. Chem. Soc., Faraday Trans. **93**, 847 (1997).
[25] Y. V. Fyodorov and H. J. Sommers, J. Math. Phys. **38**, 1918 (1997).
[26] T. Gorin, F.-M. Dittes, M. Müller, I. Rotter, and T. H. Seligman, Phys. Rev. E **56**, 2481 (1997).
[27] H. Feshbach, Ann. Phys. (N.Y.) **5**, 357 (1958); **19**, 287 (1962).
[28] U. Peskin, H. Reisler, and W. H. Miller, J. Chem. Phys. **101**, 9672 (1994).
[29] I. Rotter, J. Chem. Phys. **106**, 4810 (1997).
[30] U. Peskin, H. Reisler, and W. H. Miller, J. Chem. Phys. **106**, 4812 (1997).
[31] C. Mahaux and H. A. Weidenmüller, *Shell Model Approach to Nuclear Reactions* (North-Holland, Amsterdam, 1969).
[32] P. A. Moldauer, Phys. Rev. C **157**, 907 (1967).
[33] M. Simonius, Phys. Lett. **52B**, 17 (1978).
[34] D. Agassi, H. A. Weidenmüller, and G. Mantzouranis, Phys. Rep., Phys. Lett. **22C**, 3 (1975).
[35] V. A. Mandelshtam, H. S. Taylor, C. Jung, H. F. Bowen, and D. J. Kouri, J. Chem. Phys. **102**, 7988 (1995).
[36] T. A. Brody, J. Flores, J. B. French, P. A. Mello, A. Pandey, and S. S. M. Wong, Rev. Mod. Phys. **53**, 385 (1981).